Modelling Study of the Impact of Daily Power Modulation on Cell Thermal Balance

Mohamad Ismail[1], Bertrand Allano[2], David Munoz[3], Coralie Desages[4] and Eric Poutougnigni[5]
1. Modelling Engineer
2. Reduction Principal Advisor, Rio Expert
3. Project Manager
4. Head of process team
5. Process Engineer
Rio Tinto Aluminium Pechiney – LRF, Saint-Jean-de-Maurienne, France
Corresponding author: mohamad.ismail@riotinto.com
https://doi.org/10.71659/icsoba2024-al056

Abstract

Over the last few decades, electric power consumption has increased faster than the increase in power generation. In parallel, the increase of volatile power generation exposes us to a variation in electricity supply, which contributes to driving the prices. Flexible power is a demand-driven power management strategy, based on cost and availability of energy, that has changed the aluminium cell production rate and power consumption dynamically. This can provide benefits for both the smelting industry and the power grid, particularly as intermittent renewable energy sources become more prevalent. However, power modulation raises challenges for preserving the stability and efficiency of the smelting process, which is susceptible to temporal variations of mass, thermal and electrical balances. It is complicated to follow bath temperature variations linked to current fluctuations, given that high variation can be the primary factor for heat imbalances in the cells. In this paper, we present a new approach to follow the cell behaviour in terms of thermal balance during power modulation.

A thermo-electrical 3D transient model is used to simulate scenarios with different inputs in order to estimate the impact of power modulation on the thermal fields as well as the energy balance in the cells. This model was tested in the Laboratoire de recherches des fabrications (LRF) prototype pots to assess its predictivity and response to energy variation compared to measurements. The simulation results, for a given amperage amplitude, show an accurate prediction of the cell temperatures across various locations, particularly in the bath, and also the ledge profile variations. Moreover, this modelling enables us to estimate the temperature evolution on the cathode block surface, which allows a precise view of the cathode thermal state.

Keywords: Aluminium electrolysis, Power modulation, Thermal balance prediction, Transient model.

1. Introduction

The aluminium electrolysis process requires several hundred of thousand amperes of electricity. The aluminium industry used about 8 % of the global industrial electrical supply in 2009 [1]. In parallel, Reuters quotes (IAI) projects that by 2030, there will be a nearly 40 % increase in global demand [2]. As the prevalence of intermittent renewable energy sources has risen, this has resulted in larger fluctuations in the price and availability of electricity [3]. This represents a challenge for the smelting industry to compromise between the energy sourcing problems and increasing production costs. Usually, aluminium smelting pots run at a steady power. The response to these confrontations, linked to increasing electricity prices and the limitation of power sources, is a power modulation approach. This flexible operation allows a compatibility between

renewable energy and the electricity network, which can function as a smart grid. Power fluctuation works by overproducing when grid electricity demand is low to counteract lower production when demand is high.

The electrolysis cells can then be considered as "virtual batteries" by the electricity network. Thus, by modulating the amperage which passes through the pots according to the availability of energy on the grid, it is then possible to participate in smoothing energy consumption on the network, by optimizing aluminium production. In addition to the relative financial gains made by electrolysis plants, due to the optimization of production during off-peak periods, the common interest is also to avoid starting coal or gas power plants, to respond to peaks in demand on the network, which leads to generating high CO_2 emissions.

In past years, as early as in the 1990s, experiments related to power modulation were done in electrolysis cells in Brazil [4]. In addition, some studies were carried out where thermal and mass balance were considered in both steady and transient state [5], simulation analysis highlighted the ledge profile behaviour with manipulating some variables. Moreover, European smelters also carried out energy fluctuation tests without losing thermal control on the pots to keep heat balance and production in a stable state. To do this, retrofitting was done on a whole potline by including busbar enhancement and an addition of new heat exchangers mounted on the shell [6].

As already seen, during power modulation several aspects and physical phenomena must be carefully considered in order to ensure good control and a long lifespan of these electrolysis cells. These aspects include heat transfer, bath temperature, shell temperatures, pots thermal state and ledge profile. An increase or decrease in amperage over time, leads to a change in heat flow towards the pot sides, a variation in the bath temperature and in the liquidus temperature which influences the ledge formation [7]. The ledge is sensitive to thermal imbalance leading to melting or freezing and as a result a change in thermal and mass conditions will take place in the cell. This thermal imbalance must be anticipated and controlled before, during and after the power modulation, to maintain cell life duration and performance.

To consider these complex coupling phenomena, at Rio Tinto - LRF, we focused on the prediction of the bath temperature, and the cell thermal state during power modulation. The Flex Power project led on prototype pots allows a large set of data to be tested and analysed in order to see the capability of the thermo-electric 3D model to predict the pot thermal state.

2. Flex Power Project

The "Flex Power" program, conducted within Rio Tinto, aims to determine the possibilities of energy modulation for electrolysis plants. In other words, it is a question of determining which amperage modulation ranges are admissible by the electrolysis cells to identify necessary operational standards of operation to limit negative effect of modulations. Different 12 hours long amperage modulations are tested on prototype pots operating at 500 kA in steady-state mode. Fluctuations are about 4% from its average. Operations are done daily (change of anode, metal tapping), requiring adjustments to the resistance of the pot. These trials collect a large set of data so that it can be exploited and analysed for the need of the thermo-electric model.

2.1 Measurements Descriptions

Several thermocouples are placed on the pot side wall at different heights as shown in Figure 1. The thermocouples are linked to the Alpsys® system controlling the cell and provide real-time data [8]. The thermocouples are distributed both upstream and downstream. There are four levels of measurements aligned vertically.

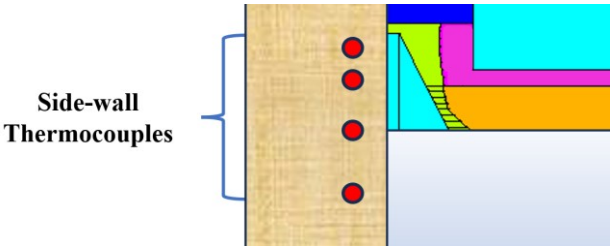

Figure 1. Thermocouple positions on the pot side walls.

One of the aims of the Flex Power project is to evaluate the impact of an amperage fluctuation on a pot. A thorough monitoring of the process parameters must be carried out, particularly for the bath temperature. So, a continuous bath temperature measurement system was put in place to collect as much data as possible. The bath temperature measurement system is located in the tap hole as seen in Figure 2.

Figure 2. Temperature measurement system position on a pot.

2.2 Measurement Analysis Method

2.2.1 Electrical Data

A normalization method of the collected data is applied to be able to use smoothed inputs in the numerical model. This method consists of choosing a stable energy modulation period and make a median of the values over this period. This allows to eliminate the non-representative points of the thermal situation due to atypical operations on the cell. This approach was applied on electrical parameters such as amperage and voltage for consecutive 24 days. The median of each hour of these 24 days is applied to obtain at the end a smooth curve over 24 hours of these 24 days, see Figure 3.

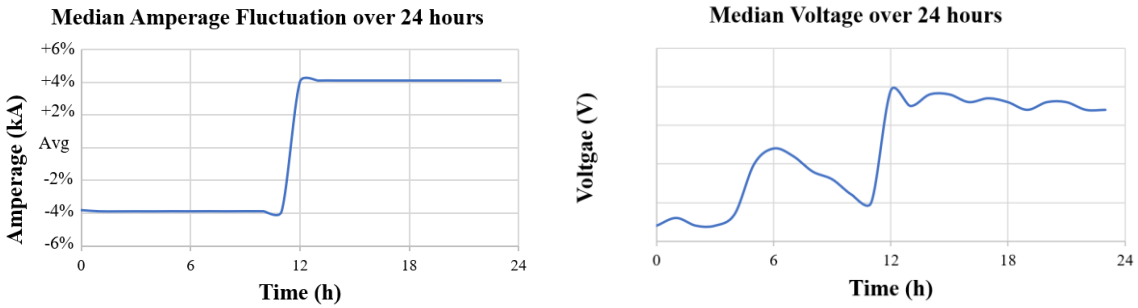

Figure 3. Left: Median method applied on electrical current measurements, Right: Median method applied on voltage measurements.

2.2.2 Bath Temperature

The continuous bath temperature data was smoothed in the same way as the measurements already mentioned. In Figure 4, it is well seen the method of collecting data each minute during 24 days of modulation. A normalized median well representing the bath temperature evolution can be seen in Figure 5.

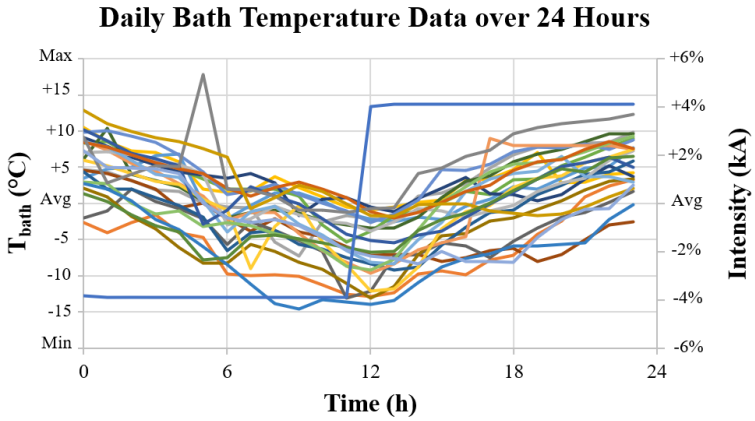

Figure 4. Bath temperature data over 24 hours.

This normalization on a global modulation cycle, shown in Figure 5, gives a median bath temperature variation, between the beginning and the end of the modulation, around 10.1 °C.

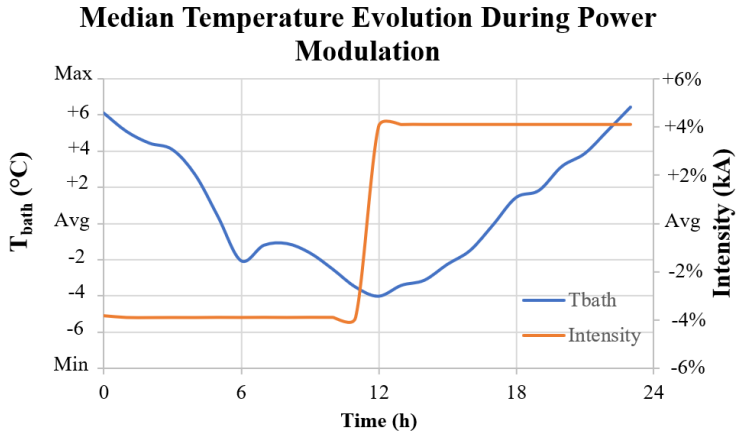

Figure 5. Median T_{bath} evolution during power modulation over 24 hours.

To follow the pot thermal state, the variation of bath temperature was also plotted in function of internal cell energy, Figure 6. Each positive or negative modulation shows an internal energy variation around 1500 kWh during the cycle. The bath temperature variation around 10.1 °C, is reversible during the modulation, there is no thermal deviation during positive/negative modulation cycles. This confirms the good conception of these amperage modulation experiments.

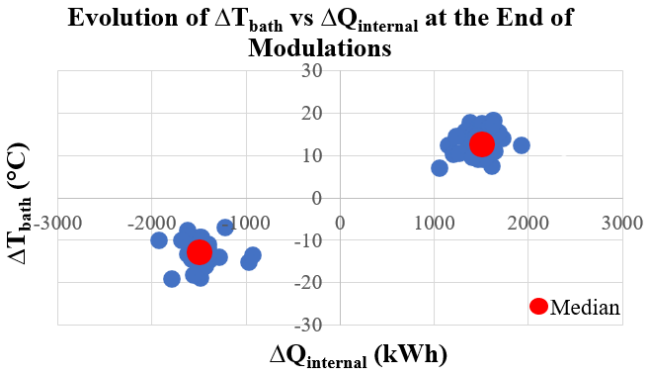

Figure 6. ΔT_{bath} vs $\Delta Q_{internal}$ at the end of modulations

Continuous bath temperature measurement shows a very good correlation with internal energy variations during modulations. Bath chemistry was taken into consideration, see Figure 7, all along of this analytical study, in order to calculate the liquidus temperature.

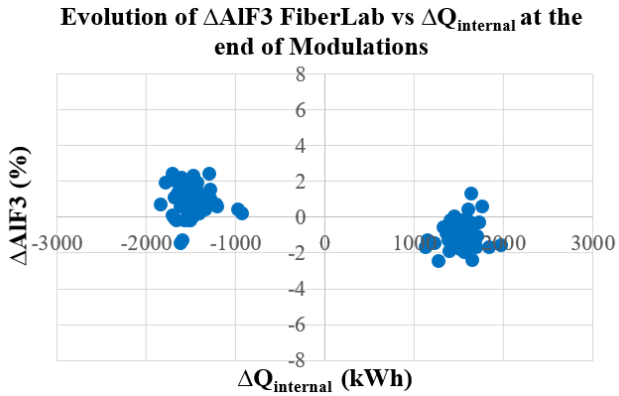

Figure 7. ΔAlF3 vs $\Delta Q_{internal}$ at the end of modulations

Monitoring liquidus temperature allows a good understanding of the superheat variation during modulations, leading to a better estimation of ledge profile state. The superheat is governed by the following formula:

$$Superheat = T_{bath} - T_{Liq} \quad (1)$$

where:

T_{bath} Bath temperature, °C

T_{Liq} Liquidus temperature, °C

3. 3D Numerical Model

To predict the thermal, electrical, and chemical effects in an electrolysis pot, the phenomena of heat transfer, electrical conduction and thermochemical reactions taking place in thermodynamic equilibrium are integrated into a thermo-electrical model. This 3D model is developed using ANSYS® software (Industrial Code in Finite Elements) and APDL language, where reduction cells may be ideally modelled using finite element analysis (FEA) techniques to better understand their behaviour and design [9]. It allows to solve differential and integral equations using 3D finite elements for solids and 2D elements for surfaces at boundary conditions. In addition, the model allows steady state and transient state studies, coupling thermo-electric analysis. It makes it possible to determine the freezing profile, the location of isotherms in the cell (anode, cathode, and lining), and the process's heat outputs [10].

3.1 Equations Representing Thermal Phenomena

In a control volume, the change in internal energy (ΔU) is equal to the amount of energy added to that system (Q) by subtracting the amount of work done by that system (W), according to the first law of thermodynamics (2):

$$\Delta U = Q - W \tag{2}$$

The concept of entropy (S) was introduced to explain both reversible systems and irreversible systems. The subsequent Equations (3-4) illustrate these reversible and irreversible transformations using the concept of entropy:

$$dS = \left(\frac{\partial Q}{T}\right)_{reversible} \tag{3}$$

$$dS > \left(\frac{\partial Q}{T}\right)_{irreversible} \tag{4}$$

The general form of a transfer equation for a scalar property ϕ is:

$$\frac{\partial \rho\phi}{\partial t} + \nabla.(\rho u\phi) - \nabla.\left(\rho\Gamma_{\phi}\nabla\phi\right) = S_{\phi}(\phi) \tag{5}$$

Heat is transferred throughout a system by thermal conduction, convection, and radiation. The phenomenon of thermal diffusion which is provoked by a temperature difference between two regions that are in direct contact or in a continuous domain, is related to conduction. Heat conduction is expressed mathematically by the following Equation (6):

$$q''_{cond} = k\frac{\partial T}{\partial X} \tag{6}$$

The convection process defined by the flow of a fluid above a surface, having different temperatures, and considers the heat transfer associated with it in Equation (7):

$$q''_{conv} = h(T_s - T_F) \tag{7}$$

Thermal radiation transmitted as an electromagnetic wave through both matter and vacuum is represented by Equation (8) by assuming that absorption is identical to emission:

$$q''_{rad} = \varepsilon\sigma(T_S^4 - T_\infty^4) \tag{8}$$

In the electrolysis cell, energy is generated in the form of Joule effect and then dissipated following the conduction laws:

$$\rho c_p\left(\frac{\partial T}{\partial t}\right) + \frac{\partial}{\partial x}\left(k_x\frac{\partial T}{\partial x}\right) + \frac{\partial}{\partial y}\left(k_y\frac{\partial T}{\partial y}\right) + \frac{\partial}{\partial z}\left(k_z\frac{\partial T}{\partial z}\right) = \dot{q} \tag{9}$$

And this heat generation via joule effect is described electrically in Equation (10):

$$\dot{q} = J.E \tag{10}$$

As the thermo-electric model calculates only the ohmic voltage drop, it's necessary to ponderate the heat generation by Joule effect in the bath with the enthalpy/tension to make metal V_{metal} and the BEMF U_{OverV}, to obtain the heat losses dissipated on the borders of the pot and the energy balance of the pot [11].

$$HL = I_{pot} \times (V_{pot} - V_{external} - V_{metal}) \quad (11)$$

Having the pot voltage:

$$V_{pot} - V_{external} = V_{anode} + V_{cathode} + V_{bath} + V_{overV} + E_{rev} \quad (12)$$

And the overvoltage's include:

$$V_{overV} = \vartheta_{anode} + \vartheta_{cathode} + \vartheta_{bubble} \quad (13)$$

Where in these equations

$\nabla.(\rho u\phi)$	Convection term
$\nabla.(\rho\Gamma_{\phi}\nabla\phi)$	Diffusion term
$S_{\phi}(\phi)$	Source term
$\frac{\partial\rho\phi}{\partial t}$	Transient term
ϕ	Scalar product
ΔU	Internal Energy Variation, J
Q	Energy added to the system, J
W	Work done by the system, J
S	Entropy, J/K
T	Temperature, K
q''	Heat flux, W/m^2
k	Thermal conductivity, W/m.K
X	Distance, m
h	Convective heat transfer coefficient, W.m^{-2}.K
T_s	Surface temperature, K
T_F	Fluid temperature, K
T_{∞}	Environmental temperature, K
ε	Emissivity
σ	Stefan Boltzmann constant, 5.67*10-8 W/m^2·K^4
$\dot{q}$	Generated energy, W/m^3
ρ	Density, kg/ m^3
t	Time, s
c_p	Heat capacity, J/kg·K
x, y, z	Directions
J	Electric current density, A/m^2
E	Electric field, V/m
H	Enthalpy, J
m	Ledge mass, kg
HL	Heat Losses, W
I	Pot amperage, kA
V_{metal}	Equivalent tension to produce metal, V
V_{pot}	Voltage of the pot, V
$V_{external}$	External voltage, V
V_{anode}	Anode Voltage drop, V
$V_{cathode}$	Cathode Voltage drop, V
V_{bath}	Bath Voltage drop, V
V_{overV}	Overvoltage's, V
E_{rev}	Equilibrium voltage, V
ϑ_{anode}	Anode overvoltage, V
$\vartheta_{cathode}$	Cathode overvoltage, V

ϑ_{bubble} Bubble overvoltage, V

3.2 Thermo-Electrical Model in Transient Mode

Steady-state heat balance is quite well understood, because of industrial expertise and widely used steady state finite elements models [12]. Solving thermo-electrical phenomena and predicting cell heat balance during power modulation needs a thermal-electrical coupled model in transient mode. At Rio Tinto – LRF, the steady state model was updated to simulate phenomena in transient mode. This model has kept the same geometry and mesh, where it is a half single-slice of electrolysis cell around one cathode block.

In steady state, it considers the methods of heat transfer both within and outside the cell, as well as the Joule effect, overvoltage, and voltage drop. The voltage distribution and the temperature are both predicted by this model. This model, which has only one slice, is lightweight and quick to execute, which makes it ideal for work on cell design and quick comparison of various options [13].

The boundary conditions applied in the model don't change:

- Current applied at the end of the rod.
- Reference voltage 0 V at the end of the cathode bars.
- Symmetry conditions are applied to the faces (centre, sides).
- Convection and radiation conditions are applied to the shell, top and bottom.

The updated transient version of this model has the capability to simulate the same physical phenomena, as in the steady state mode, through temporal dependency. The heat transfer equation described in equation (9) will be solved in transient as well. A difference in input parameters was done to introduce time-dependent amperage fluctuation scenarios, additional cell resistances for operations, forced convection network for side shell cooling, gas flow rate variation and anode-cathode distance variation.

3.2.1 Ledge Profile Detection

Ledge profile plays a major role in maintaining electrolysis pots thermal balance. The ledge dynamic behaviour is dependent upon the temperature at which the electrolyte overheats, the lining material thermal resistance, and the cryolite–alumina electrolyte composite. This process of phase changing takes place at the level of bath and metal (liquid level). Equation (7) already mentioned is responsible for the heat flow between liquid electrolyte and side ledge, where its mass change with respect to the following Equation (15):

$$\frac{\partial m_{ledge}}{\partial t} = \frac{q''_{cond} - q''_{conv}}{\Delta H_{fusion}} \quad (15)$$

Throughout power modulation ledge profile behaviour should be analysed, due to the temperature and heat flow variation.

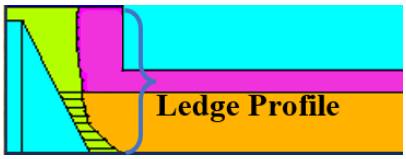

Figure 8. Ledge profile on prototype pot.

Before modelling modulations, the ledge profile is determined in a steady, average state by calculating the solid front with a gradient method from the liquidus temperature. During modulation, the initial steady ledge, the liquid bath, and the metal are modelled by using phase transition properties. When passing from steady state to transient modulations we first ensure that the ledge profile, the bath temperature, and the thermal fields are well initialized from the stationary case.

During the solidification or melting, the phase transition extends over the temperature range located below and above the temperature of the liquidus. The latent heat of transformation is the sum of the increases in enthalpy over this temperature range [14]. So, the 3D transient model takes into consideration this phase change by using the pseudo-liquid model with the integration of latent heat of fusion and the solidification of the freezing ledge. During numerical calculation, this method calculates the temperature over each single mesh. Solid phase is considered if the temperature in the mesh (bath and metal level) is lower than the liquidus temperature, then the liquid fraction will be 0, and vice versa as we can see in Figure 9.

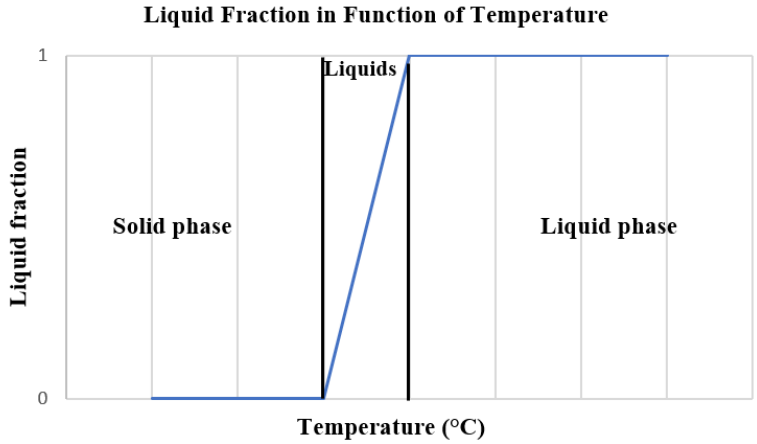

Figure 9. Liquid fraction as function of temperature.

It should be noted that the initial steady ledge profile determines the fixed position of the solid liquid conductance. This initial fixed boundary, see Figure 10 of the ledge, is taken from the stationary case calibrated over the period already mentioned.

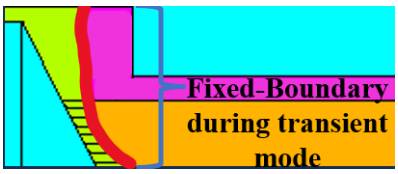

Figure 10. Fixed ledge profile during transient calculation.

4. Thermal Balance Predictions

4.1 Input Data

The measurement data were used as input in the transient thermo-electric model. This model was initiated from a tuned stationary case representing the period of the analysed modulations. Numerical calculation has been run for 72 hours to confirm the capability of the model to establish a cyclical regime and confirm that no divergence is observed during the modulation. The modulation scenario is accurately depicted by the insertion of the fluctuated current as can be seen in Figure 11.

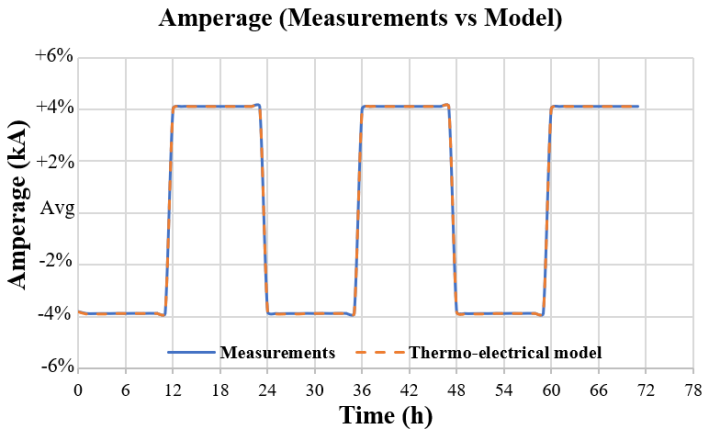

Figure 11. Current fluctuation over 72 hours.

Moreover, the additional cell resistances due to operations were calculated during the daily cycle and ably introduced. This is performed from the pot voltage and shows the great electrical impact of the operations on the pot and the physical thermal effect of these operations on the global enthalpy. In Figure 12, the simulated internal heat in the cell is presented according to the amperage modulation and to the daily operations such as anode change and tapping metal.

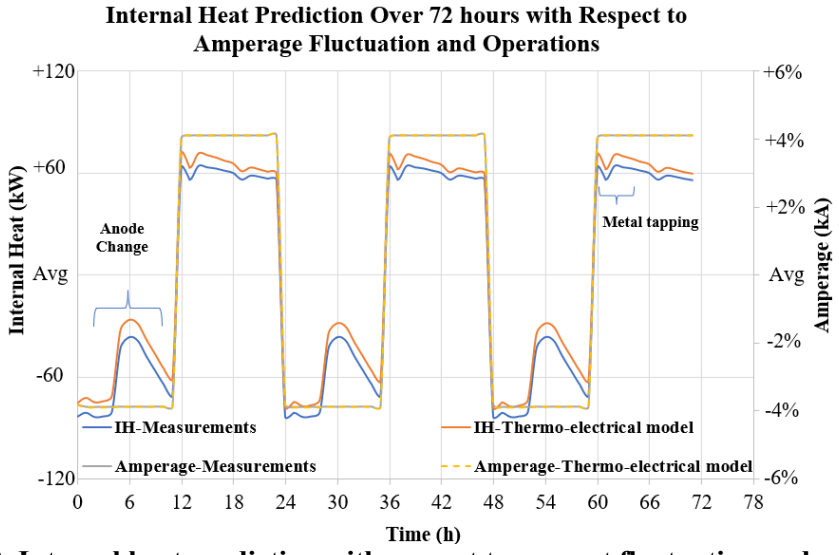

Figure 12. Internal heat prediction with respect to current fluctuation and operations.

Internal heat variation is about ± 70 kW between the beginning and the end of each modulation, where a thermal equilibrium exists. We can mention also that no drift over time is detected. The difference in the value of the starting point between the model and the measurements is due to an acceptable difference of 5 mV resulting from the calibration of the model. This led to a simple dissimilarity between the internal heat curves, as shown in Figure 12.

In this numerical study many other inputs are assumed constant, such as: forced convection network for shell cooling, Anode-cathode distance, bath chemistry, ambient temperature and the gas flow rate.

4.2 Bath Temperature Prediction

The aim of this study is to be able to predict the bath temperature and its variation to have an indicator representing the thermal state of the cell. This major indicator also affects the ledge profile and the dissipation of heat to the outside. Strong or long-term modulations can lead to thermal imbalance, pot performance deviation, and then influence the lifespan of the cell.
The transient model developed at LRF presents a good thermal response regarding the amperage fluctuations, as shown in Figure 13. Moreover, no temperature drift was observed during the time of calculation which reinforces the confidence in the transient model.

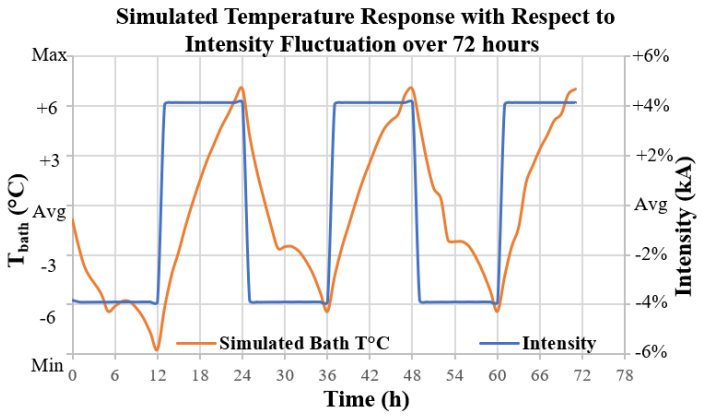

Figure 13. Numerical simulation of bath temperature and current over 72 hours.

In addition, it is showing the capability to predict the bath temperature already measured continuously, as we can see in Figure 14, a comparison between simulated and measured bath temperatures.

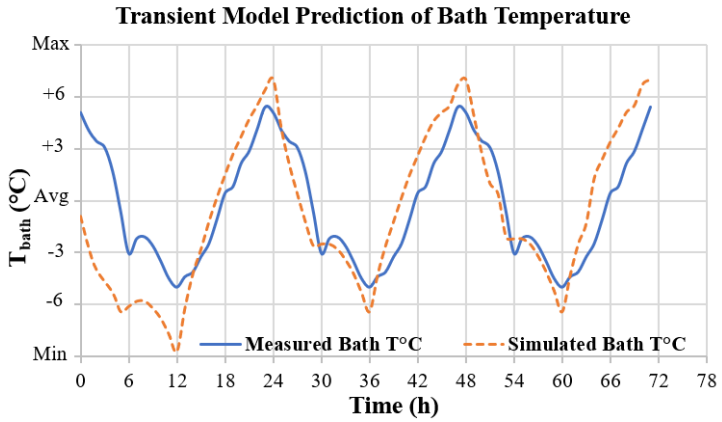

Figure 14. Bath temperature prediction by the 3D transient model.

Figure 14 demonstrates the ability of the model to predict the bath temperature with respect to the measured one. This prediction gives a variation of 12.5 °C between the end and the beginning of modulation, whereas the measured temperature variation is around 10.1 °C. This difference of 2.4 °C, between the model and the measured temperature variation, is acceptable because of the confidence in the other parameters which were not considered in transient mode. We can also notice that the initial thermal gap is recovered by the model. This gap is due to the fact that the transient model is initiated from the steady state model calibrated on an average temperature. Slopes that are well respected as seen in Figure 14, represent a good response of the model with respect to the real behaviour of the pot. So, the transient version of the TE model shows a good cyclic prediction of bath temperature.

4.3 Pot Temperatures Prediction

To confirm this prediction on all other cell temperatures, a comparison was made between the measured shell temperatures and those predicted by the model.

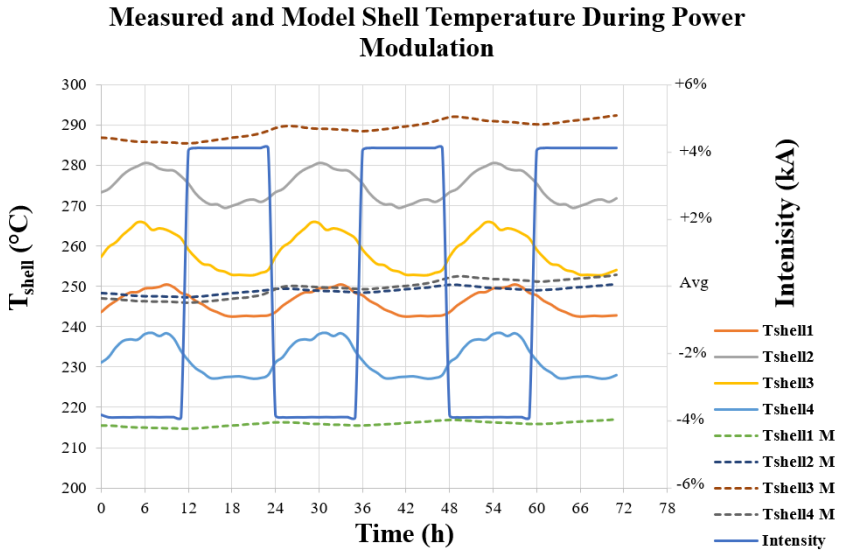

Figure 15. Measured shell temperatures vs simulated shell temperatures.

This temperature is represented by $T_{shellx}M$ for the model and T_{shellx} for measurements, where x is the vertical height. First, we can notice that the measured shell temperatures do not depend on amperage fluctuations as seen in Figure 15. Shell temperatures predicted by the model show that no significant variation exists. Secondly, to explain the variation of measured shell temperatures, it was compared with respect to the ambient temperature.

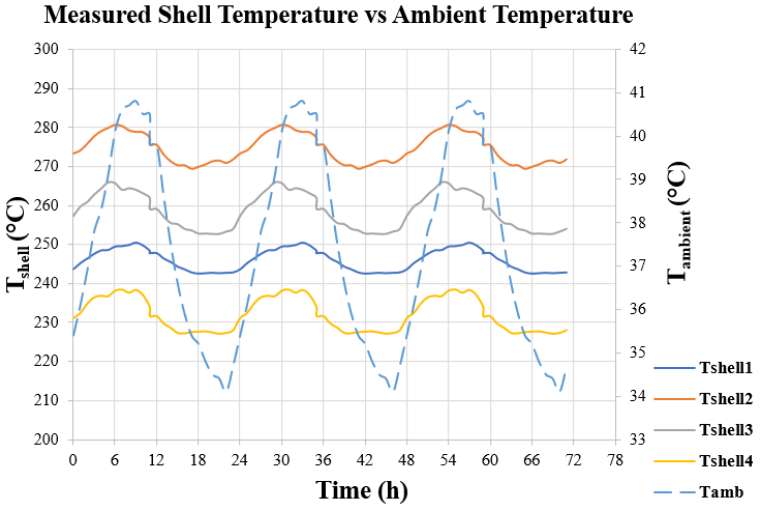

Figure 16. Measured shell temperatures vs ambient temperature.

This graph, in Figure 16, shows that the shell temperatures vary proportionally with external temperature having the same order of magnitude of 6 °C. It should be noticed that the ambient temperature was taken as constant in the numerical model. This explains the absence of shell temperature variation in the transient model. We will therefore be able to validate the thermal response of the model with respect to the modulations.

4.4 Simulated Ledge Profile

Using the transition phase method explained in section 3.2.1, the model has the capacity to separate liquid phase from solid phase by calculating the liquid fraction depending on the local liquidus temperature. To confirm that, Figure 17 shows the ledge profile detection at metal and bath level. This detection gives an overview of the pot thermal behaviour according to ledge variation.

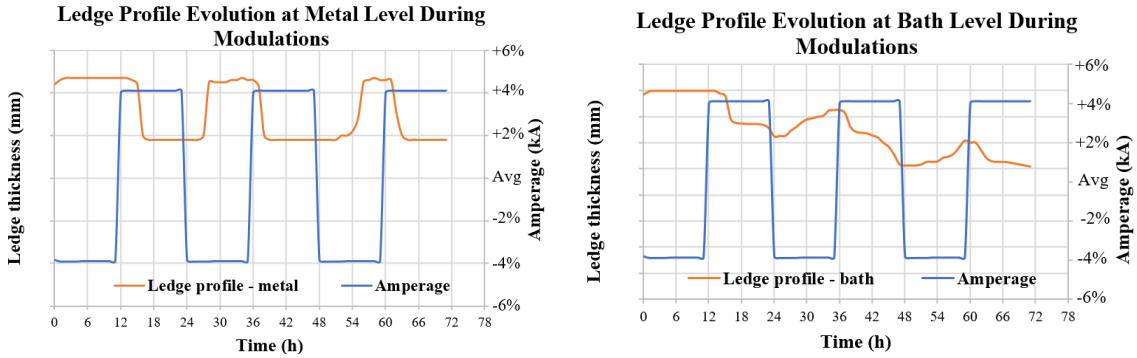

Figure 17. Ledge profile variation during current fluctuation. Left: at metal level. Right: at bath level.

Left and right sides of Figure 17 show a variation around ± 15 % of the ledge at both levels at the end of each modulation. The thickness variation is more important at the bath level. However, the melt and formation of the freezing ledge is slower at the metal level as seen in the left side. At bath level, cyclic regime is reached after 72 hours, where ledge thickness remains at the same value as at the end of the second cycle. No significant calculation drift is seen by the model hence the reliability of this detection. Established cyclic regime can be seen below, where calculation time is extended by 24 hours, Figure 18.

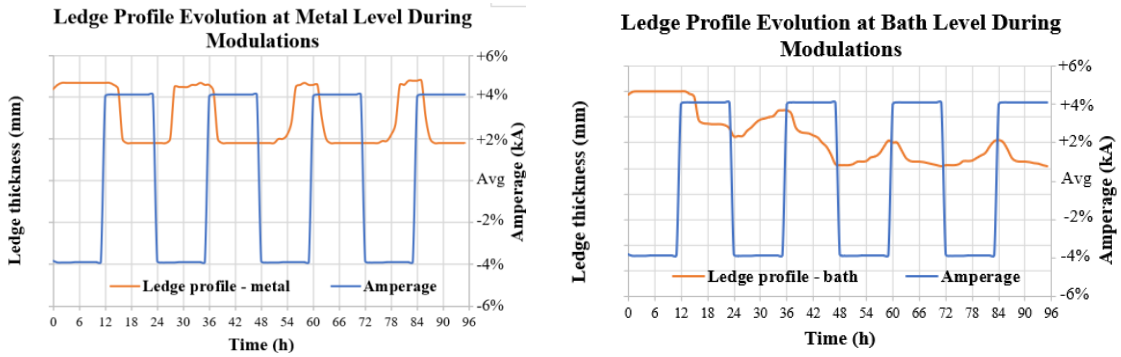

Figure 18. Ledge profile variation for 96 hours. Left: at metal level. Right: at bath level.

4.5 Thermal State of Cathode Block

A virtual sensor was developed under Ansys® to visualize the evolution of the temperature at the level of the cathode block. This evolution gives an idea of the thermal state of the block in relation to the energy fluctuation. Figure 19 shows the temperature distribution at the beginning of a high amperage fluctuation.

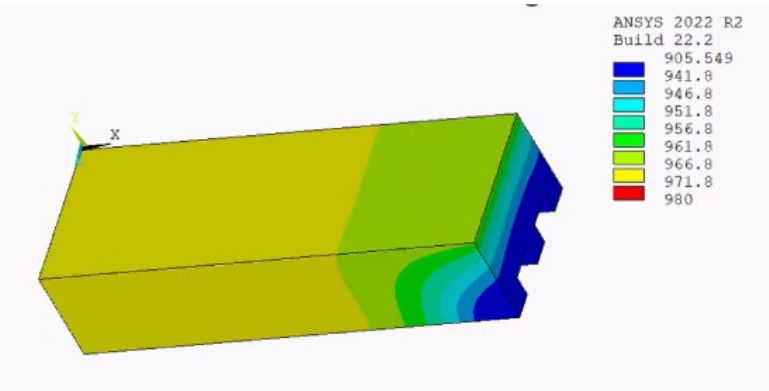

Figure 19. Temperature distribution at the cathode block.

The temperature is in the normal range, where no thermal drift was detected. A temporal video is set up to monitor the temperature evolution and the heat flow passing throughout the cathode block. In addition to that, a follow-up of the formation of ledge at the block surface was also done. Figure 20 shows the fraction curve of the cathode surface under the liquidus temperature +15 °C over the last 48 hours. This fraction could be plotted at different temperatures below, equal or higher than the liquidus temperature.

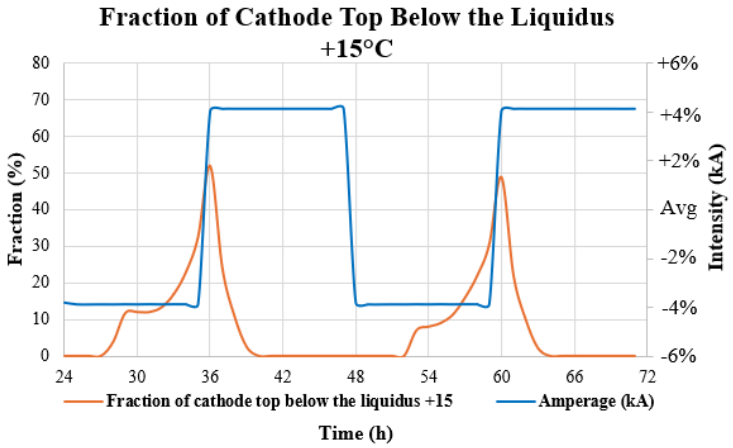

Figure 20. Fraction of cathode top below the liquidus temperature +15°C during modulations

It can be clearly seen that the cyclic representation of this variation respects the modulation. The model can predict whether the top of cathode block will freeze during low energy modulation for different scenarios and the percentage of surface covered by frozen bath.

5. Conclusions and Future Work

In this work, the “Flex Power” project at LRF is presented. A scenario of modulations was analysed after collecting a set of data. The modulations show a variation of bath temperature that should be followed to determine the reliability of modulations in smelters.

The aim of this study was to validate the ability of the thermos-electrical transient model to predict physical aspects affecting the thermal balance of an electrolysis cell.

Firstly, the model showed an accurate prediction of the bath temperature variation during power modulation. The comparison of this prediction with the analysed measurements yielded a

difference of 2.4 °C. It is mentioned also that the slopes were well respected and no thermal deviation during the simulation was detected.

Secondly, measured and predicted shell temperatures show that no variation was linked to amperage modulation. A comparison of ambient temperatures and shell temperatures evolution confirmed the interdependence between them. So, by maintaining a non-variable ambient temperature, the model ensures a good thermal response.

After these predictions, the model is able to estimate the variation of the frozen ledge profile. The numerical calculation shows a variation of the ledge well consistent with the amperage fluctuation and the temperature variation by establishing a cyclical regime at the end.

Finally, the state of the cathode block was monitored under Ansys® which showed the temperature distribution in the normal interval during the modulations. In addition, this surface is monitored by calculating the fraction of this surface below the liquidus temperature. Likewise, the model showed a cyclical regime which responds well to modulations without divergence.

As conclusion, the 3D thermo-electrical model demonstrated its ability to estimate the thermal state of the modulation scenario carried out on the prototype pots. We have considered this test was done at LRF with a successful estimation.
The next steps will be to determine the robustness of this model by testing with others pot modulation scenarios.

Future works are already in progress on a simplified physical model that can give the estimations needed, for plants wishing to start power modulations, in few minutes. This model can be implemented in the aluminium smelters which give a real time state of the thermal behaviour of the potlines.

6. References

1. Katerina Kermeli et al., Energy Efficiency Improvement and GHG Abatement in the Global Production of Primary Aluminium, *Energy Efficiency*, 8 September– 31 October 2014, vol. 8, 629-666.
2. Andy Home, Europe Adds Aluminium to its Critical Raw Materials List, *REUTERS,* https://www.reuters.com/markets/commodities/europe-adds-aluminium-its-critical-raw-materials-list-andy-home-2023-07-06/, (Accessed on 7 July 2023).
3. Dionysios P. Xenos et al., Demand-side management and optimal operation of industrial electricity consumers: An example of an energy-intensive chemical plant, *Applied Energy,* 15 November 2016, vol. 182, .418-433.
4. L.J. Pinheiro Leal Nune et al., Power Modulation on Valesul P-19 Pots, *Light Metals* 1998, 1267-1271.
5. Choon-Jie Wong et al., Studies on Power Modulation of Aluminium Smelting Cells Based on a Discretized Mass and Thermal Dynamic Model, *Metallurgical and Material Tarnsanctions B,* April 2023, Vol 54B, 562-577.
6. Roman D ussel et al., Transformation of a Potline from Conventional to a Full Flexible Production Unit, *Light Metals* 2019,533-541.
7. Olga Tkacheva et al., Solid Phase Formation During Aluminium Electrolysis, *Electrochemistry Communications,* January2020, Vol 110, 106624.
8. Nadia Chailly et al., Alucell Latest Development: Modelling Impact of CO2 Bubbles and Anode Slot Configuration on Liquid Flows in Hall-Héroult Pot, *Proceedings of 41st International ICSOBA Conference*, Dubai, 5 - 9 November 2023, *Travaux* 52, 1439-1452.
9. Imad Tabsh and Marc Dupuis, Modeling of Aluminum Reduction Cells Using Finite Element Analysis Techniques, *Light Metals*, 1995, 295-299

10. Marc Dupuis and Imad Tabsh, Thermo-Electric Coupled Field Analysis of Aluminium Reduction Cells Using the ANSYS Parametric Design Language, *Proceeding of the ANSYS® Fifth International Conference*, 1991, Vol 3, 1780-1792.
11. Kai Grjotheim, Halvor Kvande, *Introduction to Aluminium Electrolysis,* 2nd Edition, Dusseldorf, Aluminium-Verlag, 1993, 260 pages.
12. Bastien Pansiot, *Développement et qualification d'un modèle thermique électrique transitoire d'une cuve d'électrolyse d'aluminium,* Thèse de doctorat, Université de Sherbrooke, Québec, Canada, 2023
13. Yves Caratini et al., Modelling and measurements to support technological development of AP60 and APXe cells, *Proceedings of 33rd International ICSOBA Conference*, Dubai, UAE, 29 November – 1 December 2015, *Travaux* 44, 523-532.
14. Yasser Safa, *Simulation Numérique des Phénomènes Thermiques et Magnéthohydrodynamiques dans une Cellule de Hall-Héroult,* Thèse*,* Ecole Polytechnique Fédérale de Lausanne, Lausanne, 2005.